

RECIPROCATING WEAR OF IN-SITU SYNTHESIZED Ti-TiB COMPOSITES



Thesis submitted in partial fulfillment for the
Award of Degree

Doctor of Philosophy

By

Ashwani Ranjan

DEPARTMENT OF MECHANICAL ENGINEERING
INDIAN INSTITUTE OF TECHNOLOGY
(BANARAS HINDU UNIVERSITY)
VARANASI - 221005

Roll No. 15131510

2022

CERTIFICATE

It is certified that the work contained in the thesis titled "*RECIPROCATING WEAR OF IN-SITU SYNTHESIZED TI-TIB COMPOSITES*" by "*ASHWANI RANJAN*" has been carried out under our supervision and that this work has not been submitted elsewhere for a degree. A thesis submitted in partial fulfillment for the Award of Degree

It is further certified that the student has fulfilled all the requirements of Comprehensive Examination, Candidacy, and SOTA for the award of Ph.D. Degree.



Supervisor
(Prof. Rajnesh Tyagi)
IIT (BHU), Varanasi
INDIA



Co-Supervisor
(Dr. Vikas Jindal)
IIT (BHU), Varanasi
INDIA

DECLARATION BY THE CANDIDATE

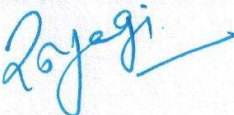
I, “**ASHWANI RANJAN**”, certify that the work embodied in this thesis is my own bonafide work and carried out by me under the supervision of “**Prof. RAJNESH TYAGI, and Dr. VIKAS JINDAL**” from “**DECEMBER 2015**” to “**NOVEMBER 2022**”, at the “**DEPARTMENT OF MECHANICAL ENGINEERING**”, Indian Institute of Technology (BHU), Varanasi, India. The matter embodied in this thesis has not been submitted for the award of any other degree/diploma. I declare that I have faithfully acknowledged and given credits to the research workers wherever their works have been cited in my work in this thesis. I further declare that I have not wilfully copied any other’s work, paragraphs, text, data, results, *etc.*, reported in journals, books, magazines, reports dissertations, theses, *etc.*, or available at websites and have not included them in this thesis and have not cited as my own work.


Date: 29/11/2022
Place: Varanasi



(**ASHWANI RANJAN**)

CERTIFICATE BY THE SUPERVISORS

It is certified that the above statement made by the student is correct to the best of our knowledge.


Supervisor
(Prof. Rajnesh Tyagi)
IIT (BHU), Varanasi
INDIA


Co-Supervisor
(Dr. Vikas Jindal)
IIT (BHU), Varanasi
INDIA


Signature of Head of Department
यान्त्रिक अभियान्तिकी विभाग / Deptt. of Mechanical Engg.
भारतीय प्रौद्योगिकी संस्थान / Indian Institute of Technology
वाराणसी / Varanasi (B.H.U.)
221005 / Varanasi-221005

COPYRIGHT TRANSFER CERTIFICATE

Title of the Thesis: Reciprocating Wear of In-situ Synthesized Ti-TiB Composites

Name of the Student: Ashwani Ranjan

Copyright Transfer

The undersigned hereby assigns to the Indian Institute of Technology (Banaras Hindu University), Varanasi all rights under copyright that may exist in and for the above thesis submitted for the award of the **Doctor of Philosophy**.

Date:

29/11/2022

Place:

Varanasi



(Ashwani Ranjan)

Note: However, the author may reproduce or authorize others to reproduce material extracted verbatim from the thesis or derivative of the thesis for the author's personal use provided that the source and the Institute's copyright notice are indicated.

ACKNOWLEDGEMENT

The author is pleased to express his sincere thanks and gratitude beyond words to his supervisor Prof. Rajnesh Tyagi and co-supervisor Dr. Vikas Jindal for their consistent help, encouragement and valuable discussions during the entire period of his research work. The author would not have been able to complete the thesis without their utmost involvement and invaluable efforts. They motivated the author to pursue research problems and the need for persistent effort to accomplish the goal. The author is truly indebted to them.

Besides supervisors, the author would like to thank his RPEC members, Prof. Sunil Mohan and Prof. R. K. Gautam for their insightful comments and encouragement. The author acknowledges his deep sense of gratitude to the current and former Heads of the Department of Mechanical Engineering for providing all the research facilities to accomplish his research in the Department successfully. The author has an immense sense of gratitude to all the faculty members of the Department of Mechanical Engineering, IIT (BHU), Varanasi for their cooperation and inspiration.

The author is grateful to all his friends, Ms. Pooja Verma, Mr. Nitish Mahto, Mr. Abhay Kumar, and seniors, especially Mr. Rohit Kumar Singh Gautam, for their constant encouragement, making joyful and memorable life being with him in moments of happiness and difficulties at IIT (BHU), Varanasi. The author is also thankful to all the lab and office staff of the department, especially Mr. Vijay Pratap Srivastava (CAM lab).

The author would also like to express his immense gratitude to his parents Smt. Prema Devi and Shri Pramod Kumar Pandey, Sister Shilpi Kumari, Madav Pandey,

The author would also like to express his immense gratitude to his parents Smt. Prema Devi and Shri Pramod Kumar Pandey, Sister Shilpi Kumari, and Madav Pandey, for their unconditional support and encouragement, to pursue his interest. The author also wishes to thank all those who have helped in any manner during the course of his research work.

At last thanks to the almighty God who has given the author spiritual support and courage to carry out this work.



(ASHWANI RANJAN)

TABLE OF CONTENTS

<i>CONTENTS</i>		Page No.
<i>LIST OF FIGURES</i>		Xii
<i>LIST OF TABLES</i>		Xix
<i>LIST OF ABBREVIATIONS/SYMBOLS</i>		Xx
<i>ABSTRACT</i>		Xxi
Chapter 1	INTRODUCTION	1
Chapter 2	REVIEW OF LITERATURE	
2.1	COMPOSITE AND ITS TYPES	5
2.1.1	DESIGN AND PROCESSING TECHNIQUES FOR COMPOSITES	6
2.1.1.1	LIQUID STATE PROCESSING	7
2.1.1.2	SOLID STATE PROCESSING	8
2.1.1.3	VAPOUR AND GAS PHASE DEPOSITION	11
2.1.1.4	IN-SITU PROCESSING	13
2.2	VACUUM ARC MELTING	14
2.3	TRIBOLOGY	15
2.4.	WEAR AND TYPES OF WEAR	16
2.4.1	FACTORS AFFECTING WEAR	17
2.5	TITANIUM BASED COMPOSITES AND THEIR MECHANICAL PROPERTIES	20

2.6	DRY SLIDING OF WEAR OF TITANIUM-BASED COMPOSITES	29
2.6.1	CONTAINING TiB PHASE IN Ti MATRIX	30
2.7	FORMULATION OF THE PROBLEM	36
2.8	OBJECTIVES OF STUDY	37
Chapter 3	EXPERIMENTAL PROCEDURE	
3.1	MATERIALS USED	39
3.2	FABRICATION OF COMPOSITES	41
3.2.1	MIXING OF POWDERS	41
3.2.2	SPARK PLASMA SINTERING	42
3.2.3	VACUUM ARC MELTING	43
3.3	CHARACTERISATION OF COMPOSITES	45
3.3.1	X-RAY DIFFRACTION ANALYSIS OF COMPOSITES	45
3.3.2	HARDNESS MEASUREMENT	46
3.3.3	POROSITY MEASUREMENT	46
3.4	MICROSTRUCTURAL EXAMINATION	46
3.5	DRY SLIDING FRICTION AND WEAR TESTING	47
3.6	EXAMINATION OF WORN SURFACES	49
3.6.1	HIGH-RESOLUTION SCANNING ELECTRON MICROSCOPY(HR-SEM)	50
3.6.2	X-RAY DIFFRACTION ANALYSIS	51
Chapter 4	Ti-TiB-Fe COMPOSITES WITH VARYING AMOUNT OF Fe	

4.1	RESULTS: Ti-TiB-Fe COMPOSITES WITH VARYING AMOUNT OF Fe	52
4.1.1	CHARACTERIZATION OF COMPOSITES	52
4.1.2	FRICITION AND WEAR BEHAVIOR OF COMPOSITES	56
4.1.3	EXAMINATION OF WORN SURFACE OF COMPOSITES	59
4.1.4	WORN SURFACE MORPHOLOGY OF COUNTERFACE	62
4.1.5	EXAMINATION OF WEAR DEBRIS	65
4.2	DISCUSSION	66
4.3	RESULTS: Ti-TiB-Fe COMPOSITES WITH VARYING AMOUNT OF B	69
4.3.1	CHARACTERIZATION OF COMPOSITES	69
4.3.2	FRICITION AND WEAR BEHAVIOR OF COMPOSITES	71
4.3.3	EXAMINATION OF WORN SURFACE OF COMPOSITES	73
4.3.4	EXAMINATION OF WORN SURFACE OF COUNTERFACE	77
4.3.5	EXAMINATION OF WEAR DEBRIS	79
4.4	DISCUSSION	81
Chapter 5	RECIPROCATING WEAR BEHAVIOUR OF Ti-TiB COMPOSITES SYNTHESIZED VIA VACUUM ARC MELTING	
5.1	RESULTS	84
5.1.1	CHARACTERIZATION OF POWDERS	84
5.1.2	CHARACTERIZATION OF COMPOSITES	85
5.1.3	FRICITION AND WEAR BEHAVIOR OF COMPOSITES	88

5.1.4	WORN SURFACE MORPHOLOGY OF COMPOSITES	92
5.1.5	WORN SURFACE MORPHOLOGY OF COUNTERFACE	97
5.1.6	MORPHOLOGY OF DEBRIS	102
5.1.7	XPS ANALYSIS OF DEBRIS	103
5.2	DISCUSSION	105
5.3.1	FRICITION AND WEAR BEHAVIOR OF COMPOSITES	110
5.3.2	WORN SURFACE MORPHOLOGY OF COMPOSITE	114
5.3.3	WORN SURFACE MORPHOLOGY OF COUNTERFACE	118
5.3.4	EXAMINATION OF WEAR DEBRIS	121
5.4	DISCUSSION	123
5.5	RESULTS	125
5.5.1	RECIPROCATING WEAR OF COMPOSITES AT 10Hz	128
5.5.2	EXAMINATION OF WORN SURFACE OF COMPOSITE	129
5.5.3	EXAMINATION OF WORN SURFACE OF COUNTERFACE	133
5.5.4	EXAMINATION OF DEBRIS	137

5.6	DISCUSSION	139
5.7	RESULTS	140
5.7.1	RECIPROCATING WEAR OF COMPOSITES AT 15Hz	141
5.7.2	EXAMINATION OF WORN SURFACE OF COMPOSITE	144
5.7.3	EXAMINATION OF WORN SURFACE OF COUNTERFACE	149
5.7.4	EXAMINATION OF DEBRIS	152
5.8	DISCUSSION	154
Chapter 6	CONCLUSIONS	159
<i>FUTURE SCOPE</i>		167
<i>REFERENCES</i>		168
<i>LIST OF PUBLICATIONS</i>		177

LIST OF FIGURES

Figure 2.1	Matrix-based classification of Composites. (Rosso et al., 2006)	6
Figure 2.2	Classification of the processing routes to develop MMCs	7
Figure 2.3	Steps involved in the powder Metallurgy process	7
Figure 2.4	A schematic diagram of sintering (Ayatimur et al., 2014)	10
Figure 2.5	Schematic diagram of co-deposition of a metallic matrix and reinforcing particulates via thermal spray process (Asthana et al., 2015).	11
Figure 2.6	Schematic diagram of Spark plasma sintering of powder sample (Guyot et al 2012)	13
Figure 2.7	Classification of the design and processing routes to develop specific properties in MMCs	22
Figure 3.1	Schematic diagram of a typical spark plasma sintering machine	44
Figure 3.2	General arrangement of Arc melting equipment 1. Arc Torch 2. Powder melting copper hearth 3. Gutter 4. Control handle 5. Arc Power Source 6. Argon gas inlet 7. Water cooling system	46
Figure 3.3	Schematic diagram of the reciprocating ball on disk testing	51
Figure 4.1	XRD pattern of as prepared composites (a) TiBFe1010 (b) TiBFe1020 (c) , and TiBFe1030	55
Figure 4.2	Scanning electron micrographs showing the microstructure of composites (a) TiBFe1010, (b) TiBFe1020, and (c) TiBFe1030 (d) Micrograph of composite TiBFe 1030 used for color mapping, and (e, f, g) show the presence Ti, B, and Fe, respectively	56
Figure 4.3	Variation of coefficient of friction with time for TiBFe1010, TiBFe1020, and TiBFe1030 composites at different loads (a) 10 N, (b) 15 N, (c)20 N, and (d) 25 N	58
Figure 4.4	Variation of average coefficient of friction (a) load and (b) composites Fe (at.%)	59

Figure 4.5	Variation of wear rate of the composites TiBFe1010, TiBFe1020, and TiBFe1030 with (a) load and (b) composites Fe (at.%)	60
Figure 4.6	SEM images of worn surfaces of composite at a load of 10 N (a) TiBFe1010 (b) TiBFe1020 and (c) TiBFe1030	62
Figure 4.7	SEM images of worn surfaces of composite at a load of 15 N (a) TiBFe1010 (b) TiBFe1020 and (c) TiBFe1030	62
Figure 4.8	SEM images of worn surfaces of composite at a load of 20 N (a) TiBFe1010 (b) TiBFe1020 and (c) TiBFe1030	63
Figure 4.9	SEM images of worn surfaces of composite at a load of 25 N (a) TiBFe1010 (b) TiBFe1020 (c) TiBFe1030 and (d) EDS of TiBFe1030	63
Figure 4.10	Worn surfaces of bearing steel ball slid against (a) TiBFe1010 (b) TiBFe1020 (c) TiBFe1030 composite at a load of 10N	64
Figure 4.11	Worn surfaces of bearing steel ball slid against (a) TiBFe1010 (b) TiBFe1020 (c) TiBFe1030 composite at a load of 15N	64
Figure 4.12	Worn surfaces of bearing steel ball slid against (a) TiBFe1010 (b) TiBFe1020 (c) TiBFe1030 composite at a load of 20N	65
Figure 4.13	Worn surfaces of bearing steel ball slid against (a) TiBFe1010 (b) TiBFe1020 (c) TiBFe1030 composite at a load of 25N	65
Figure 4.14	SEM micrographs of wear debris (a) TiBFe1010 at 10N (b) TiBFe1020 at 10N (c) TiBFe1030 at 10N (d) TiBFe1010 at 25N (e) TiBFe1020 at 25N (f) TiBFe1030 at 25N (g) EDS analysis of grey and white spots of Fig.8(d)	66
Figure 4.15	XRD pattern of the wear debris collected after the wear tests	67
Figure 4.16	XRD pattern of as prepared composites (a) TiBFe1010 (b) TiBFe2010 and (c) TiBFe3010	71
Figure 4.17	Scanning electron micrographs showing microstructure and mapping of composites (a–d) TiBFe1010, (e–h) TiBFe2010, and (i–l) TiBFe3010, respectively	72
Figure 4.18	Variation of coefficient of friction with time for TiBFe1010, TiBFe2010 and TiBFe3010 composite at different loads (a) 10 N, (b) 15 N, (c) 20 N and (d) 25 N	74

Figure 4.19	Variation of average coefficient of friction with (a) load and (b) Composition	75
Figure 4.20	Variation of wear rate with (a) load and (b) Composition	75
Figure 4.21	SEM images of worn surfaces of composite at a load of 10N (a) TiBFe1010 (b) TiBFe2010, and (c) TiBFe3010	77
Figure 4.22	SEM images of worn surfaces of composite at a load of 15 N (a)TiBFe1010 (b) TiBFe2010, and (c) TiBFe3010	77
Figure 4.23	SEM images of worn surfaces of composite at a load of 20N (a) TiBFe1010 (b) TiBFe2010, and (c) TiBFe3010	77
Figure 4.24	SEM images of worn surfaces of composite at a load of 25N (a) TiBFe1010 (b) TiBFe2010, and (c) TiBFe3010	78
Figure 4.25	Worn surfaces of bearing steel ball slid against (a) TiBFe1010 (b) TiBFe2010 and (c) TiBFe3010 composite at a load of 10N	79
Figure 4.26	Worn surfaces of bearing steel ball slid against (a) TiBFe1010 (b) TiBFe2010 and (c) TiBFe3010 composite at a load of 15N	80
Figure 4.27	Worn surfaces of bearing steel ball slid against (a) TiBFe1010 (b) TiBFe2010 and (c) TiBFe3010 composite at a load of 20N	80
Figure 4.28	Worn surfaces of bearing steel ball slid against (a) TiBFe1010 (b) TiBFe2010 and (c) TiBFe3010 composite at a load of 25N	80
Figure 4.29	SEM micrographs of wear debris (a) TiBFe1010 at 10N load (b) TiBFe2010 at 10N load (c) TiBFe3010 at a load of 10 N	81
Figure 4.30	SEM micrographs of wear debris (a) TiBFe1010 at 25N load (b) TiBFe2010 at 25N load (c) TiBFe3010 at a load of 25 N	81
Figure 4.31	XRD spectra of the debris	82
Figure 5.1	SEM micrographs of feedstock powder (a) Ti and (b) TiB ₂	84
Figure 5.2	XRD pattern of composites (a)Ti, (b)TiB50, (c) TiB60, (d) TiB70, (e) TiB80, and (f) TiB85	85
Figure 5.3	Scanning electron micrographs (a-k) and BSE images (l-q) showing microstructure of composites (a) pure Ti, (b) TiB50, (c) TiB60, (d) TiB70,(e) TiB80, (f) TiB85,and elemental distribution of TiB70 (g-j), (k) Magnified region showing blocky and whiskers	86

	nature of TiB in composite TiB85, (l) pure Ti, (m) TiB50, (n)TiB60, (o) TiB70, (p)TiB80, (q) TiB85.	
Figure 5.4	Variation of coefficient of friction with time for 10,15,20, and 25 N (a)Ti,(b)TiB50, (c)TiB60, (d) TiB70, (e)TiB80, and (f) TiB85 composites at different loads	89
Figure 5.5	Variation of average coefficient of friction (a) load and (b) composites TiB (Vol.%).	91
Figure 5.6	Variation of wear rate of the composites with (a) load and (b) composites TiB (vol.%)	91
Figure 5.7	SEM images of worn surfaces of composite at a load of 10 N (a)Ti, (b) TiB50, (c) TiB60, (d) TiB70, (e) TiB80, (f) TiB85, and (g) EDS of worn surface for TiB50	93
Figure 5.8	SEM and EDS of worn surfaces of composite at a load of 15 N (a)Ti, (b) TiB50, (c) TiB60, (d) TiB70, (e) TiB80 and, (f) TiB85	93
Figure 5.9	SEM images of worn surfaces of composite at a load of 20 N (a)Ti, (b) TiB50, (c) TiB60, (d) TiB70, (e) TiB80 and, (f) TiB85	95
Figure 5.10	SEM images and EDX of worn surfaces of composite at a load of 25 N (a)Ti, (b) TiB50, (c) TiB60, (d) TiB70, (e) TiB80 and, (f) TiB85	96
Figure 5.11	SEM images of worn surfaces of bearing steel ball at a load of 10 N(a)Ti, (b) TiB50, (c) TiB60, (d) TiB70, (e) TiB80, and (f) TiB85	97
Figure 5.12	SEM images of worn surfaces of bearing steel ball at a load of 15 N (a)Ti, (b) TiB50, (c) TiB60, (d) TiB70, (e) TiB80 and, (f) TiB85	98
Figure 5.13	SEM images of worn surfaces of bearing steel ball at a load of 20 N (a)Ti, (b) TiB50, (c) TiB60, (d) TiB70, (e) TiB80 and, (f) TiB85	99
Figure 5.14	SEM and EDS images of worn surfaces of bearing steel ball at a load of 25 N (a)Ti, (b) TiB50, (c) TiB60, (d) TiB70, (e) TiB80 and, (f) TiB85	100
Figure 5.15	SEM and EDS images of worn surfaces of pooled debris (a)Ti, (b) TiB50, (c) TiB60, (d) TiB70, (e) TiB80, and (f) TiB85	101
Figure 5.16	XRD spectra of the debris	102
Figure 5.17	High resolution XPS spectra of pooled debris of composites (a) full XPS spectra (b) B 1s, (c) Ti 2p and (d) Fe 2p	103
Figure 5.18	Variation of coefficient of friction with time for 10 N, 15 N, 20 N, and 25N at 7 Hz of different composites (a) Ti, (b) TiB50, (c) TiB60,	110

	(d)TiB70, (e) TiB80, and (f) TiB85	
Figure 5.19	Variation of average coefficient of friction with (a) load and (b) Composition	111
Figure 5.20	Variation of wear rate with (a) load and (b) Composition	112
Figure 5.21	SEM images of worn surface of TiB composite (a)Ti, (b) TiB50, (c) TiB60 (d)TiB70 (e) TiB80, and (f) TiB85 at 7 Hz and 10 N	113
Figure 5.2	SEM images of worn surface of TiB composite (a)Ti, (b) TiB50, (c) TiB60 (d)TiB70 (e) TiB80, and (f) TiB85 at 7 Hz and 15 N	114
Figure 5.23	SEM images of worn surface of TiB composite (a)Ti, (b) TiB50, (c) TiB60 (d)TiB70 (e) TiB80, and (f) TiB85 at 7 Hz and 20 N	115
Figure 5.24	SEM and EDS images of worn surface of TiB composite (a)Ti, (b) TiB50, (c) TiB60 (d)TiB70 (e) TiB80, and (f) TiB85 at 7 Hz and 25 N	116
Figure 5.25	SEM images of worn surface of counterface ball (a)Ti, (b) TiB50 (c) TiB60 (d)TiB70 (e) TiB80, and (f) TiB85 at 7 Hz and 10 N	117
Figure 5.26	SEM images of worn surface of counterface ball (a)Ti, (b) TiB50 (c) TiB60 (d)TiB70 (e) TiB80, and (f) TiB85 at 7 Hz and 15 N	119
Figure 5.27	SEM images of worn surface of counterface ball (a)Ti, (b) TiB50 (c) TiB60 (d)TiB70 (e) TiB80, and (f) TiB85 at 7 Hz and 20 N	120
Figure 5.28	SEM micrograph of worn surface of counterface ball (a)Ti, (b) TiB50(c) TiB60 (d)TiB70 (e) TiB80, and (f) TiB85 at 7 Hz and 25 N	120
Figure 5.29	SEM micrograph of pooled debris of (a)Ti, (b)TiB50, (c) TiB60, (d)TiB70, (e) TiB80, and (f) TiB85 at 7 Hz	121
Figure 5.30	XRD spectra of the debris	121
Figure 5.31	Variation of coefficient of friction with time for 10, 15, 20, and 25 N(a) Ti(b) TiB50, (c) TiB60, (d) TiB70, (e) TiB80, and (f) TiB85 composites at different loads	125
Figure 5.32	Variation of average coefficient of friction with (a) load and, (b) Composition	127

Figure 5.33	Variation of wear rate with (a) load and, (b) Composition	128
Figure 5.34	SEM images of worn surfaces of composite at a load of 10 N (a)Ti, (b) TiB50, (c) TiB60, (d) TiB70, (e) TiB80 and, (f) TiB85	130
Figure 5.35	SEM images of worn surfaces of composite at a load of 15 N (a)Ti, (b) TiB50, (c) TiB60, (d) TiB70, (e) TiB80 and, (f) TiB85	131
Figure 5.36	SEM images of worn surfaces of composite at a load of 20 N (a)Ti, (b) TiB50, (c) TiB60, (d) TiB70, (e) TiB80 and, (f) TiB85	131
Figure 5.37	SEM images of worn surfaces of composite at a load of 25 N (a)Ti,(b) TiB50, (c) TiB60, (d) TiB70, (e) TiB80 and, (f) TiB85	132
Figure 5.38	SEM images of worn surface of bearing steel ball slid against TiB composite (a) Ti, (b)TiB50, (c) TiB60, (d)TiB70, (e) TiB80, and (f) TiB85 at10 Hz and 10N	135
Figure 5.39	SEM images of worn surface of bearing steel ball slid against TiB composite (a) Ti (b)TiB50, (c) TiB60, (d)TiB70, (e) TiB80, and (f) TiB85 at10 Hz and 15 N	135
Figure 5.40	SEM images of worn surface of bearing steel ball slid against TiB composite (a) Ti (b)TiB50, (c) TiB60, (d)TiB70, (e) TiB80, and (f) TiB85 at10 Hz and 20 N	136
Figure 5.41	SEM images of worn surface of bearing steel ball slid against TiB composite (a) Ti, (b)TiB50, (c) TiB60, (d)TiB70, (e) TiB80, and (f) TiB85 at10 Hz and 25 N	136
Figure 5.42	SEM images of pooled debris form bearing steel ball slid against TiB composite (a) Ti, (b) TiB50, (c) TiB60 (d)TiB70, (e) TiB80, and (f) TiB85 at 10 Hz	137
Figure 5.43	XRD spectra of the debris	138
Figure 5.44	Variation of coefficient of friction with time for 10, 15, 20, and 25 N (a)Ti,(b)TiB50, (c)TiB60, (d) TiB70, (e)TiB80, and (f) TiB85 composites at different loads.	141
Figure 5.45	Variation of average coefficient of friction with (a) load and (b) Composition	143
Figure 5.46	Variation of wear rate of friction with (a) load and, (b) Composition	143
Figure 5.47	SEM images of worn surface TiB composite slid against bearing steel ball(a) Ti, (b) TiB50, (c) TiB60, (d)TiB70, (e) TiB80, and (f) TiB85 at 15 Hz and 10 N	145

Figure 5.48	SEM images of worn surface TiB composite slid against bearing steel ball (a) Ti, (b) TiB50, (c) TiB60, (d)TiB70, (e) TiB80, and (f) TiB85 at 15 Hz and 15 N	146
Figure 5.49	SEM images of worn surface TiB composite slid against bearing steel ball(a) Ti, (b) TiB50, (c) TiB60, (d)TiB70, (e) TiB80, and (f) TiB85 at 15 Hz and 20 N	146
Figure 5.50	SEM and EDS images of worn surface TiB composite slid against bearing steel ball(a) Ti, (b) TiB50, (c) TiB60, (d)TiB70, (e) TiB80, and (f) TiB85 at 15 Hz and 25 N	148
Figure 5.51	SEM images of counterface steel ball(a) Ti, (b) TiB50, (c) TiB60, (d)TiB70,(e) TiB80, and (f) TiB85 at 15 Hz and 10 N	150
Figure 5.52	SEM images of counterface steel ball(a) Ti, (b) TiB50, (c) TiB60, (d)TiB70, (e) TiB80, and (f) TiB85 at 15 Hz and 15 N	150
Figure 5.53	SEM images of counterface steel ball(a) Ti, (b) TiB50, (c) TiB60, (d)TiB70, (e) TiB80, and (f) TiB85 at 15 Hz and 20 N	151
Figure 5.54	SEM images of counterface steel ball(a) Ti, (b) TiB50, (c) TiB60, (d)TiB70, (e) TiB80, and (f) TiB85 at 15 Hz and 25 N	151
Figure 5.55	SEM images of counterface steel ball(a) Ti, (b) TiB50, (c) TiB60, (d)TiB70, (e) TiB80, and (f) TiB85 at 15 Hz and 10 N	152
Figure 5.56	XRD patterns of wear debris at 15 Hz	152
Figure 5.57	Average coefficient of friction of Ti and Ti-TiB composites at different frequencies and loads	156
Figure 5.58	Wear rate of Ti and Ti-TiB composites at different frequencies and loads	157

LIST OF TABLES

Table 3.1	Chemical composition of titanium (Ti) powder and titanium diboride TiB ₂	42
Table 3.2	Composite designation and composition (at. %) of B and Fe	42
Table 3.3	Composite designation and composition (wt. %) of powders	43
Table 3.4	Arc produced for synthesis parameters	47
Table 3.5	Experimental conditions and equipment used for friction and wear testing.	52
Table 4.1	Designation, Hardness, and Porosity of composites	56
Table 5.1	Designation, Hardness, Density, and Porosity of composites	87

LIST OF ABBREVIATIONS/SYMBOLS

μ	:	Coefficient of friction
$^{\circ}\text{C}$:	Degree Celsius
γ	:	Delta
EDS	:	Energy-dispersive X-ray spectroscopy
g	:	Gram
H	:	Hardness of softer materials
HR-SEM	:	High resolution scanning electron microscopy
Hr	:	Hour
θ	:	Incident angle
n	:	Integer representing order of the diffraction
d	:	Interplanar spacing
K	:	Kelvin
MPa	:	Mega Pascal
μm	:	Micrometer
min	:	Minute
N	:	Normal load
%	:	Percentage
RPM	:	Revolution per minute
m	:	Sliding distance
s	:	Sec
T	:	Temperature
HV	:	Vickers hardness
V	:	Volume loss
λ	:	Wavelength of the x-ray
K	:	Wear coefficient
SEM	:	Scanning electron microscopy
W	:	Wear volume loss
wt.%	:	Weight percentage
XRD	:	X- ray diffraction

ABSTRACT

The term “Tribology” was coined in 1966, which deals with the study of interacting surfaces in relative motion and encompasses the phenomena of friction, and wear. The technological significance of the field can be gauged by the fact that most machine failures are caused by the wear of machine elements, which renders them unsuitable to perform their intended function and necessitates their replacement. Wear is the most common cause of material waste and loss of mechanical performance, and any reduction in wear can result in significant economic savings. Friction is a major source of wear and energy loss. Improved friction control is expected to result in significant cost savings. It is estimated that one-third of the world's current energy resources are required to overcome friction in some form or another.

Titanium Matrix Composites (TMCs) combine favorable mechanical properties, good corrosion resistance, and high-temperature durability. Due to the excellent corrosion resistance, low density, appropriate mechanical properties, and high biocompatibility, titanium, and its alloys are widely used in the chemical, submarine, aeronautical, and biomedical industries. However, the relatively low hardness and poor wear resistance restrict their applications in the components where wear is a problem. A number of Ti matrix composites (TMCs) containing different hard phases as the reinforcements are being fabricated and researched to overcome this. This class of MMCs have are attractive and a lot of attention is being paid towards their development because of (a) the availability of different types of reinforcement at reasonable prices, (b) the successful development of manufacturing processes to produce MMCs with reproducible structure and properties, and (c) the availability of standard or near-standard metal

working methods that can be used to fabricate these MMCs.

The present study has been conducted to investigate the tribological behavior of Ti-based composites containing different Vol.% of TiB synthesized via vacuum arc melting technique, by performing dry sliding reciprocating wear tests at different loads and frequencies. Further, looking into the present trend of research, the present study also envisages unraveling the friction and wear behavior of titanium-based composites containing different Vol.% of TiB. The composites containing different amounts of TiB have been synthesized at the same sintering temperatures to determine the optimum TiB Vol.% based on the examination of their mechanical properties and tribological performance. Titanium-based composites containing different contents of TiB_w have been prepared at this optimized sintering Vol.% and their friction and wear characteristics may be evaluated under different working conditions to explore the effect of reinforcement content on the coefficient of friction and wear rate. Pure titanium-based composites containing different amounts of TiB_w have also been prepared and tested under similar conditions for the purpose of comparison taking pure Ti as the base sample. The study also intends to establish the prevailing mechanisms of wear under the conditions used in the investigation for this new class of composites.

The thesis has been organized in the following six chapters:

Chapter 1 contains the introductory remarks highlighting the technological importance of the problem under investigation.

Chapter 2 provides a critical review of the published literature on composites and their tribological properties. It begins with a brief description on the composites and their processing techniques, with a special focus on vacuum arc melting which has been used in the present study. This is followed by a description on tribology, the various types

of wear and the parameters that affect the phenomenon of wear including a brief overview of the fundamentals of friction and some basic friction and wear theories. The chapter also covers the details of the studies conducted for synthesizing the Ti-based composites containing different second-phase reinforcements and the evaluation of their mechanical properties. A detailed description of the friction and wear behavior of Ti-TiB composites also forms a part of this chapter. The chapter also presents the gap in the published research, which has helped in the formulation of the problem and ends with the objectives of the present study.

Chapter 3 outlines the details of experimental procedures followed in the current investigation. In the present study, the metal powders used for making the sample were Ti powder (99.4% pure; average particle size of 100 μm ; Alfa Aesar, USA), TiB₂ powder (99.5% pure; average particle size of 325 μm ; Alfa Aesar, USA), Fe (99.7% pure; average particle size of 6 μm ; Thermo Fisher Scientific, USA). Two sets of composites have been synthesized using two different routes i.e., spark plasma sintering (SPS) and vacuum arc melting (VAM). In the first set five composites have been varying fabricated by varying Fe (at a fixed B at. %) and Boron (at a fixed Fe at. %) content from 10-30 at.%, and are designated as TiBFe1010 (10% B and 10 % Fe), TiBFe1020 (10 % B and 20 % Fe), TiBFe1030 (10 % B and 30 % Fe), TiBFe2010(20 % B and 10 % Fe) and TiBFe3010 (30% B and 10% Fe). In another set, Ti-TiB composites containing five different volume percentages of TiB (50, 60, 70, 80, and 85 Vol.%) have been prepared by vacuum arc melting and are designated as TiB50, TiB60, TiB70, TiB80, and TiB85. Pure Ti specimens have also been prepared using the same process for the purpose of comparison. X-ray diffractometer and high resolution-scanning electron microscope (HR-SEM) equipped with energy dispersive spectroscopy have been used to characterize the composites. The details of the procedure used for tribo-testing of composites along

with various parameters are also included in the chapter. All the tests have been performed using a Linear Reciprocating Ball-on-Flat Sliding Wear configuration against a counterface of bearing steel ball at different loads (10, 15, 20, and 25 N), with a stroke length of 1 mm at 5 Hz and at a frequency (4, 7, 10, and 15 Hz) with a stroke length 2mm according to ASTM G133. The chapter also provides the details of techniques like SEM, XRD and Raman spectroscopy used for the analysis of worn surfaces and wear debris of all the composites and counterface ball.

Chapter 4 begins with the presentation of results on the structure and property characterization of TiTiBFe composites, i.e., TiBFe1010, TiBFe1020, TiBFe1030, TiBFe2010, and TiBFe3010 synthesized via spark plasma sintering, namely XRD patterns of composite reveal the peaks corresponding to the presence of TiB phase FeTi, and Ti, which indicate that there is no oxidation of the powders during sintering. A dense and compacted structure with a higher volume fraction of TiB and FeTi was observed. The hardness of the composite increases with the increase of both FeTi and TiB phases but with TiB phases the hardness value is high. in comparison to 30 wt.% Fe as measured by a Vickers hardness.

The chapter also contains the results and discussion pertaining to the friction and wear characteristics of TiBFe1010, TiBFe1020, TiBFe1030, TiBFe2010, and TiBFe3010 composites. The results on tribological performance have been evaluated by carrying out reciprocating wear tests at different loads of 10, 15, 20, and 25 N and a fixed frequency of 5 Hz, and results are presented in two parts: (i) TiBFe1010, TiBFe1020, TiBFe1030 composites having fixed Boron and varying Fe and (ii) TiBFe1010, TiBFe2010, and TiBFe3010 containing fixed Fe but varying amount of B. All the composites i.e., TiBFe1010, TiBFe1020, TiBFe1030, TiBFe2010, and TiBFe3010 have been observed to possess a typical microstructure containing β -Ti, TiB and intermetallic

FeTi. The hardness of the composites increased from 488 to 871 HV_{0.1} with the addition of Fe from 10 to 30 at. %, which has been attributed to the increasing amount of the formation of FeTi. The coefficient of friction decreased with an increasing amount of Fe at each of the loads i.e., 10, 15, 20, and 25 N, and the composite containing 30 at. % Fe, i.e., TiBFe1030 showed the lowest coefficient of friction. However, wear rate decreased with increasing Fe content from 10 to 20 at. % followed by an increase again for 30 at. % addition at each of the loads. The lowest wear rate was observed for TiBFe1020 having 20 at. % Fe despite its lower hardness than TiBFe1030 and has been attributed to dominating effect of the transfer layer present over the sliding surface which shields the underlying substrate from direct metal-metal contact. The hardness of composites containing 10 to 30 at. % B at a fixed amount of Fe increased from 488 to 964 HV_{0.1}. The composite TiBFe3010 showed the lowest coefficient of friction (between 0.51 and 0.44) and wear rate (TiBFe3010) with increasing load (ranging from 0.41 - 1.32 x10⁻⁴ mm³/m) due to increasing TiB content. The dominating mechanisms for have been found to be delamination and ploughing as revealed by morphologies of the worn surfaces.

Chapter 5 describes the results of the structure and property characterization of Ti-TiB campsites synthesized via vacuum arc melting. Ti-TiB composites have been prepared by varying the TiB₂ wt.% in the Ti matrix to get different volume fractions of TiB, namely TiB50, TiB60, TiB70, TiB80, and TiB85. XRD patterns of composite reveal the peaks corresponding to the presence of TiB phase and Ti, indicating that melting of powders occurred without any oxidation or disintegration. The SEM micrographs of the microstructure of TiB50, TiB60, TiB70, TiB80, and TiB85 composites revealed relatively dense structures with two different shapes of TiB (i) whiskers and (ii) blocky in the Ti matrix. However, the composites with higher volume fraction of TiB were observed to be denser than lower volume fraction composites. The hardness has been observed to

increase with an increase in TiB content in the composites i.e., 256 HV for pure Ti to 895 HV for TiB85.

The chapter also contains the results and discussion pertaining to the friction and wear characteristics of Ti, TiB50, TiB60, TiB70, TiB80, and TiB85 composites at different loads (10, 15, 20 and 25 N) and frequencies (4, 7, 10 and 15 Hz). The coefficient of friction (COF) has been found to fluctuate with time with relatively larger fluctuations in amplitude for all the composites in comparison to pure Ti. The composites have shown a run-in period having larger fluctuations before attaining a steady state. The duration of run-in period at a fixed frequency has been observed to depend on the composition and the load. However, the variation of coefficient of friction is observed to be steady for Ti at all loads with almost no running-in stage. The steady state coefficient of friction has not shown any particular trend of variation with load and composition at all frequencies i.e., 4, 7, 10, and 15 Hz. Both the coefficient of friction and wear rate increased with increasing load for all the composites. At a given load, the coefficient of friction and the wear rate of the composites decreased from 50 to 60 Vol.% TiB followed by an increase for 70 Vol.% and a reduction thereafter till 80 Vol.% and remained almost the same thereafter till 85 Vol.% TiB.

The average coefficient of friction for Ti, TiB50, TiB60, TiB70, TiB80, and TiB85 composites has been found to decrease with increasing load with the exception of Ti, which has shown an increase in coefficient of friction from 10 to 25 N a frequency of 7 Hz. However, TiB80 has shown a lower COF at all the loads in comparison to TiB50, TiB60, TiB70, and TiB85 with a minimum COF of 0.40 and maximum COF of 0.51 at 10 N. The observed behavior has been attributed to the presence of a transfer layer of oxides of debris over the surface which prevents direct contact between mating bodies and provides easy shearing junctions at the interface. The variation of wear rate with load

did not shown any particular trend in composites whereas it has been observed to increase with increasing load for pure Ti. The wear rate of TiB50 increased from 10 to 15 N then decreased till 25 N. TiB60 showed an increase in wear rate from 10 to 20 N thereafter decreased a little at 25 N, while TiB70, TiB80 and TiB85 showed similar trends i.e. their wear rate increased from 10 N to 15 N followed by a decrease till 25 N with a minimum value of $0.18 \times 10^{-4} \text{ mm}^3/\text{m}$. This has been attributed to the formation of a well compacted transfer layer and its degree of compaction which prevents the wear of the underlying substrate. The operative mechanism of wear has been found to be a mixture of ploughing, adhesion, and oxidation for pure Ti whereas the same for composites is adhesion, oxidation, delamination, and abrasion for all loads and frequencies.

The average coefficient of friction for pure Ti, TiB50, TiB60, TiB70, TiB80, and TiB85 decreased with increasing load from 10 to 25 N for a frequency of 10 Hz. The composite TiB80 showed the lowest COF among all and pure Ti showed the highest. The wear rate of pure Ti increased with increasing load Ti and it had the highest wear rate among all the materials. The composites did not reveal any specific trend of variation of wear rate with load. Among all composites, TiB80 demonstrated the lowest wear rate and the observed behavior has been attributed to the presence of a transfer layer containing lubricious of oxides. The mechanism of wear is observed to be a combination of a ploughing, abrasion, and oxidation for Ti and whereas the same for composites was a mix of delamination, abrasion, adhesion, and oxidation. However, at a frequency of 15 Hz, the average COF is found to increase with increasing load for pure Ti whereas it is observed to either decrease of remain constant for composites with increasing load. TiB80 showed the lowest coefficient of friction at all the loads. At relatively lower loads of 10 and 15 N pure Ti also showed almost same COF as TiB80. The wear rate did not show any specific trend of variation with load for at 15 Hz also. The wear rate decreased with

an increase in load for TiB60, TiB80, and TiB85 whereas for TiB50 and TiB70 it decreased from 10 to 15 N followed by an increase at 20 N before decreasing further at 25 N. The wear rate shown by pure Ti is significantly higher in comparison to composites which reflects the effect of the addition of TiB. Among all the composites, TiB85 composite has shown the lowest rate of wear at all the loads and the lowest rate of $0.23 \times 10^{-4} \text{mm}^3/\text{m}$ is observed at 25 N. This has been attributed to the formation of a well compacted transfer layer and its degree of compaction which prevents the wear of the underlying substrate. The mechanism of wear for composite is a mixture of ploughing, abrasion, adhesion and oxidation whereas for Ti ploughing, delamination and oxidation are the primary mechanisms of wear.

The composite having 80 Vol.% TiB showed the lowest coefficient of friction and wear rate among all the composites at 4, 7, and 10 Hz due to the formation of a transfer layer of wear debris over the surface, its degree of compaction, and the presence of lubricious oxides (TiO_2 , B_2O_3 , and H_3BO_3) as revealed by XPS. Whereas, at 15 Hz, TiB85 has shown a marginally lower coefficient of friction and wear rate among all composites.

Chapter 6 presents the major conclusions of the present study pertaining to the microstructure and properties of composites along with their friction and wear characteristics under different loads, and frequency and the role of TiB in extending the effect of titanium matrix composites.